Li-LSX-zeolite evaluation for post-combustion CO2 capture

Accepted Manuscript

Li-LSX-zeolite evaluation for post-combustion CO_2 capture

Rasmus Kodasma, Javier Fermoso, Aimaro Sanna

PII: S1385-8947(18)32002-3
DOI: https://doi.org/10.1016/j.cej.2018.10.063
Reference: CEJ 20126

To appear in: *Chemical Engineering Journal*

Received Date: 16 May 2018
Revised Date: 5 October 2018
Accepted Date: 8 October 2018

Please cite this article as: R. Kodasma, J. Fermoso, A. Sanna, Li-LSX-zeolite evaluation for post-combustion CO_2 capture, *Chemical Engineering Journal* (2018), doi: https://doi.org/10.1016/j.cej.2018.10.063

Title page

Li-LSX-zeolite evaluation for post-combustion CO_2 capture

Author names and affiliations

Rasmus Kodasma, Javier Fermoso, Aimaro Sanna*

Institute of Mechanical, Process and Energy Engineering, School of Engineering and Physical Sciences, Heriot-Watt University, Edinburgh EH14 4AS, UK

Corresponding author*:

Phone: +44(0)1314518108. *E-mail address:* a.sanna@hw.ac.uk (Aimaro Sanna). Institute of Mechanical, Process and Energy Engineering, School of Engineering and Physical Sciences, Heriot-Watt University, EH14 4AS, Edinburgh, UK

Abstract

Lithium low silica X type (Li-LSX) zeolite is typically used for industrial N_2/O_2 separation processes, but its potential as a carbon dioxide capture sorbent has not been fully evaluated yet. In this work, Li-LSX zeolite was investigated as CO_2 sorbent under post- combustion conditions in TGA and Fixed-bed configurations. The maximum adsorption capacity and CO_2/N_2 selectivity were determined to be 4.43 mmol g^{-1} and 85.7 at 60ºC and in presence of 14% CO_2, using a packed bed configuration. The CO_2 and N_2 adsorption capacity was decreased of 10 mol% when the initial calcination temperature was raised from 60 to 300ºC due to a decreased micropore surface. However, the high calcination temperature increased the CO_2 selectivity to 128.1 and increased the adsorption rates due to enhanced basicity (1 order of magnitude) and external surface (+75-80%) in the Li-LSX zeolite.

The sorption stability at 60ºC was found to be excellent during 85 sorption cycles over 35 hour period with Li-LSX showing negligible difference in adsorption capacity throughout the cycles and a working capacity of 2.45 mmolCO_2/g after an initial calcination at 550°C (2 min) and cyclic adsorption at 60°C (6 min) and desorption at 420°C (5 min). The Avrami kinetic model shows the coexistence of different adsorption mechanisms. CO_2 adsorption rate increased with the increasing CO_2 partial pressure, as a result of the facilitated CO_2 diffusion processes. Film diffusion was determined as the rate-limiting step for CO_2 adsorption. Therefore, based on these findings, Li-LSX represents a promising sorbent for post-combustion carbon capture.

Keywords: Carbon capture and storage, CO_2 solid adsorbent, zeolite, Li-LSX-zeolite.

1. Introduction

In order to ensure future climate stability, it is of a crucial importance to develop economically viable technologies to limit anthropogenic carbon emissions (the concentration of CO_2 in the atmosphere has exceeded 407 ppm threshold in June 2018 [1], in a world still highly dependent on fossil fuels based technologies. The majority of anthropogenic carbon dioxide emissions come from heavy emitting industries such as the coal, steel and cement sectors. Carbon capture and storage (CCS) is considered to be the most viable technology for reducing CO_2 emissions from these sectors [2].

A range of carbon capture technologies exist today – as of 2018, monoethanolamine (MEA) is the most mature post-combustion carbon capture technology. However, it also presents several disadvantages such as: high solvent regeneration penalty, corrosiveness and its potential negative impact on human health and the environment [3]. In order to overcome amine-based carbon capture technology shortcomings, there has been an increasing interest in the application of solid sorbents for carbon capture via adsorption process [4]. Solid sorbents technology has the potential to reduce the cost per tonne of CO_2 captured from £50-60 for MEA to £30-£40 [5].

Numerous solid sorbent materials have been previously investigated, and the most important ones include metal organic frameworks (MOFs), zeolites, hydrotalcites, activated carbons and mesoporous silica materials [6]. As an example, mono and triamine tethered MCM-41 adsorbents exhibited a maximum adsorption capacity of 1.2 and 2.1 mmol g^{-1} (75ºC, 0.2 bar), respectively [7]. A good adsorbent should possess high CO_2 selectivity and adsorption capacity, low heat of adsorption, high thermal and mechanical stability, stable cyclic adsorption capacity, production scalability and low cost [5,8]. Zeolites have shown to have

the highest sorption performance metrics of the second generation of carbon capture materials under post-combustion conditions [9].

Selectivity is one of the most important properties for solid sorbent materials considered for large-scale applications. Materials that do not yield a high separation factor between carbon dioxide and nitrogen will necessitate the use of additional downstream CO_2 purification, which adds to the already high capital and operating costs of the carbon capture plant [8]. Due to its high counter-ion concentration and a high surface area, which are correlated with high selectivity and adsorption capacity respectively, zeolite Li-LSX (lithium low silica X zeolites) has been the preferred sorbent for air separation in pressure swing adsorption processes. Leonova and Mel'gunov [10] studied the physisorption of CO_2 and N_2O using LSX and Li/H modified LSX zeolites at 0ºC using TGA and found their CO_2 adsorption properties favourable, especially their good CO_2/N_2O adsorption selectivity up to 0.007 bar at 0ºC. Moreover, Chen et al. [11] synthesized a novel LiPdAgX zeolite, which showed some of the best selectivity performance up to date, with a separation factor of 61 at 10% CO_2 concentration.

Impregnation of zeolites is also being investigated to improve adsorption characteristics, especially selectivity. In this way, Mohamedali et al., [9] reported that ZIF-8 zeolites impregnated with 30% ionic liquid (1-Butyl-3-methylimidazolium Acetate) exhibited substantially higher CO_2 uptake and CO_2/N_2 selectivity at temperatures ranging 30 – 50ºC than the original ZIF-8; in particular, the capacity at 0.2 bar and 30ºC was 0.83 mmol g^{-1}, i.e. 7 times higher than the pristine ZIF-8.

In 2017, NASA investigated the use of zeolites CO_2 sorbents for deep space exploration using a packed bed reactor [12]. Among notable candidates, Li-LSX zeolite had a surprisingly high CO_2 adsorption capacity with 9.5 wt% at 25ºC using a gas containing 0.5 vol% CO_2 (pre-adsorption calcination at 350ºC). Similarly, Stuckert and Yang [13], have shown that Li-LSX

zeolite is a good candidate for the removal of CO_2 from the atmosphere. Li-LSX was found to have double the capacity of zeolite NaX at atmospheric conditions, also higher than all other reported zeolites, with 0.82 mmolCO_2 g^{-1}, using 395 ppm CO_2 in air at 25ºC.

Incorporation of Li^+ and H^+ resulted in a significant decrease of adsorption selectivity towards CO_2 in a pressure range 0.01 – 1 Torr compared to the initial LSX in the K-Na form. This feature allowed simultaneous quantitative sequestration of CO_2 and N_2O traces from contaminated gas flows. Under pressures just below atmospheric pressure, the selectivity CO_2/N_2O reached 1.0 and the total uptake (at 0ºC) came close to the uptake of N_2O (around 120 ml g^{-1}) [10]. Moreover, it has been shown that the uptake of pure CO_2 in X and LSX type zeolites was compromised due to a decrease of the electric field gradients decreased, so that CO_2 was less prone to adsorb [14].

The adsorption performance of Li-LSX has also been shown to decrease with the presence of water moisture [14]. Their results indicated that the Henry constants for CO_2 adsorption declines exponentially with the loading of water hence leading to poor adsorption performance with flue gases high in water content.

The literature available on the use of Li-LSX zeolites for CO_2 sorption indicates a lack of knowledge for its application as post-combustion sorbent under conditions typical of coal power stations and other industrial emitters such as cement and steel plants. More specifically, there is a lack of data concerning: comprehensive evaluation of carbon capture parameters such as adsorption capacity, rate, selectivity and adsorption kinetics at various CO_2 concentrations corresponding to post- and pre-combustion conditions and little data exists on Li-LSX carbon capture performance in a scaled up fixed-bed reactor. Furthermore, there is potential for calculating the economic parameters for Li-LSX as a carbon capture sorbent to investigate whether its use in scaled up carbon capture applications would be economically viable.

Therefore, this work aims to fill in the outlined gaps in literature and to give a comprehensive analysis of Li-LSX performance in terms of (i) CO_2 adsorption capacity, (ii) adsorption/desorption rates, (iii) breakthrough curves, (iv) kinetics, (v) selectivity and (vi) cyclic adsorption-desorption studies.

2. Materials and methods

2.1. Materials

Li-LSX zeolite (HYGB100C) was acquired from Shanghai Hengye Chemical Industry Co. Ltd. in spherical pellet form (1.6-2.5 mm) All the pure gases (CO_2, N_2 and He) with a purity > 99.99 vol%, as well as the 14 vol% CO_2 (in N_2 balance) were supplied by BOC (UK). Specific gravity (1.92 g/cm^3), particle size (12-200mesh).

2.2. Characterisation methods

2.2.1. BET analysis

Physical properties were analysed using a Micromeritics Gemini VII 2390 Surface Area Analyser. The sample (0.5 g) was outgassed at 200ºC for 12 h before running the N_2 physisorption isotherms at −195ºC. The surface area was determined by using the standard Brunauer–Emmett–Teller (BET) equation using a low pressure region of 13 points from 0.01 to 0.25 relative pressure. One point pore volume was obtained at a relative pressure of 0.984. Micropore volume, micropore area and external surface area were calculated by T-Plot, while the mesopore volume and pore width were calculated using DFT (NLDFT/QSDFT). A BET test was carried out using CO_2 instead of N_2, to evaluate the CO_2 uptake at 0°C. The same method as above was used, but with the difference that a water-ice bath was used instead of liquid nitrogen.

2.2.2. Mass spectroscopy (MS)

A Quadrupole Mass Spectrometer (MKS-Cirrus 2) was used to analyse either the gas composition of feeding gases (inlet) or the outlet gas streams coming from the TGA and fixed-bed reactor. The MS data were processed using Process Eye Professional software. A 2m long silica capillary inlet heated to 150ºC and with a vacuum flow rate of 20 ml min^{-1} was used for sampling the gases.

2.2.3. X Ray Diffraction analysis (XRD)

The Powder X-Ray Diffraction (XRD) analysis of the zeolite was carried out on a Bruker Nonius X8-Apex2 CCD diffractometer equipped with an Oxford Cryosystems Cryostream (typically operating at 100 K), and an X-ray source with a Cu anode working at 40 kV and 40 mA and an energy-dispersive one-dimensional detector. Raw data were converted by PowDLL Converter and the identification and quantification of crystalline phases were carried out by QualX 2.23 software, which supported a reference pattern database derived from Crystallography Open Database (COD).

2.3. Thermogravimetric analysis

A thermogravimetric analyser TGA (Q500, TA Instruments) was employed to test both the adsorption capacity and reaction rate of Li-LSX zeolite at atmospheric pressure. For the experiments, about 30 mg of the zeolite were loaded in the Pt crucible, and the total gas flow rate was varied from 35 to 100 ml min^{-1} depending on the experiment, while the adsorption temperature ranged from 40 to 250ºC. In the same way, the initial calcination temperature varied from 60 to 550°C, depending on the experiment. A number of experiments were carried out using diluted flue gas (X vol% CO_2; Y vol% N_2 (or He), while other were run using pure N_2 or CO_2.

Different temperature programmes were used in the TGA experiments. The first step of TGA experiments was a pre-desorption to remove from the zeolite sample any CO_2, H_2O or impurity, in which the sample was heated at 50ºC min^{-1} up to 550ºC under 50 ml min^{-1} N_2

flow rate and held for 15-50 min, depending on the experiment. After that, the sample temperature was cooled down to the selected adsorption temperature in the same atmosphere. Once the adsorption temperature become stable, the gas stream was switched to CO_2 gas at 5-16 ml min^{-1} (depending on the experiment) and held for 6-40 minutes (depending on the experiment) in order to get a steady plateau in the sample weight saturation. After that, for the desorption step, the gas was switched again to N_2 50 ml min^{-1} and the temperature increased to 420-550ºC at a rate of 25-50ºC min^{-1} in order to desorb the gas from the zeolite. These steps were consecutively repeated in certain experiments.

The basicity of Li-LSX zeolite after different calcination temperatures was run using the following method: potential adsorbed species in the catalysts were removed by heating in Helium at 50°C/min to 550°C and holding the final temperature for 50 min. Then, the temperature was decreased to 60°C and CO_2 flushed in the TGA for 30 minutes for allowing its adsorption on the catalysts surface. Then, the gas in the TGA was switched back to Helium at 60°C and for 20 min, to allow the physiosorbed CO_2 to be desorbed. Finally, the temperature was ramp to 600°C at 10°C/min to determine the chemisorbed CO_2.

To evaluate the performance of the Li-LSX zeolite over cycles, a test was carried out repeating the adsorption/desorption steps for 85 times after an initial calcination at 550ºC (2 min at temperature). For this particular experiment, a flow of 14 vol% CO_2 (balanced with N_2 for a total of 100 ml min^{-1}) a heating rate of 50ºC min^{-1}, adsorption at 60ºC (6 min) and desorption at 420ºC (5 min) were used to simulate a "fast adsorption/desorption cycle.

The adsorption or desorption capacity expressed in mmolCO_2 $g^{-1}_{zeolite}$ were calculated using the following equation by using the total weight sample change (*wt%*) during the adsorption or desorption steps:

$$\text{Capacity}\left(\text{mmol CO}_2\ \text{g}_{\text{zeolite}}^{-1}\right) = \frac{\text{wt\%}\cdot\left(\frac{1\ \text{g CO}_2}{100\ \text{g}_{\text{zeolite}}}\right)\cdot\left(\frac{1000\ \text{mg CO}_2}{1\ \text{g CO}_2}\right)}{44\frac{\text{mg CO}_2}{\text{mmol CO}_2}} \qquad \text{Eq. 1}$$

The CO_2 adsorption rate (Ads rate) was calculated from the maximum value of the first derivative curve of the weight sample change during the adsorption with time (min) from the following expression:

$$\text{Ads rate (mmol CO}_2\text{ min}^{-1}) = \left(\frac{\text{wt\%}_i - \text{wt\%}_{i-1}}{t_i - t_{i-1}}\right)\left(\frac{\left(\left(\frac{1\text{ g CO}_2}{100\text{ g}_{\text{zeolite}}}\right)\right)\left(\frac{1000\text{ mg CO}_2}{1\text{ g CO}_2}\right)}{44\frac{\text{mg CO}_2}{\text{mmol CO}_2}}\right) \quad \text{Eq. 2}$$

where, $wt\%_i$ would represent the sample weight percentage at time any t_i (in min).

The CO_2/N_2 and CO_2/H_2O separation factors (selectivity) from the TGA and fixed-bed results were calculated according to the following equation.

$$\text{Selectivity to CO}_2 = \frac{\frac{\text{CO}_2\text{ adsorbed (mmol CO}_2\text{ g}^{-1})}{\text{j adsorbed (mmol j g}^{-1})}}{\frac{\text{vol\% CO}_2}{\text{vol\% j}}} \quad \text{Eq. 3}$$

where *j* represents either N_2 or water.

2.4. Kinetic analysis and adsorption mechanism modelling

In order to investigate the CO_2 adsorption kinetics, mechanism of adsorption and predicting the rate-controlling steps, CO_2 adsorption experimental data obtained at different temperatures in presence of 14 vol% and 100 vol% CO_2 were analysed using several kinetic models including the pseudo firs order and second order kinetic models, the Elovich model and the Avrami model. The linear equations of the models available in literature were used to obtain the kinetic parameters [15-17]. In the pseudo-first order kinetic model, which represent a reversible interaction between adsorbent and adsorbate typically used to predict physical adsorption of CO_2 on solid sorbents, the plot of log(qe-qt) vs time (t) produces a linear function, where the slope and intercept are (k1/2.303) and (log qe), respectively. The pseudo second order constant, which has been found suitable to predict CO_2 sorption behaviour based on chemical interactions, is obtained by plotting (t/qt) vs t, which results in a linear function where the slope and the intercept represent (1/qe) and (qe^2/k2), respectively. The Elovich

model states that the rate of adsorption exponentially decreases with time, due to the increase of CO_2 surface coverage. A graph of (qt) vs (ln(t)) produces a linear plot where the slope and the intercept are ((1/β) and (1/β)ln(αβ)), respectively [17]. Finally, the Avrami's fractional order kinetic model of particle nucleation ($dqt/dt=Ka^{na}t^{na-1}(qe-qt)$), previously tested for CO_2 adsorption was also evaluated [18]. In this latest model, ka is the Avrami kinetic constant and na is the Avrami exponent reflecting mechanism changes that may take place during the adsorption process [19].

The above models integrate all the mass transfer resistances to adsorption such as external diffusion, pore diffusion and surface adhesion [19]. To give insight on the rate controlling steps associated with the CO_2 adsorption kinetics, the intra-particle diffusion kinetic model and the Boyd model were used [16,19]. The intra-particle diffusion model describes the stepwise adsorption process of adsorbate over adsorbent surface, where the overall adsorption mechanism can be controlled by film diffusion, external diffusion, surface diffusion or a combination of these steps. The intraparticle diffusion rate constant is obtained plotting (qt) vs (t^0.5), which yields a linear function in which (k) and (C) are the slope and intercept, respectively. Boyd's diffusion model was used to predict the diffusion phenomenon regulating the interactions between the adsorbate and the adsorbent [16].

The models were validated based on the value of coefficient of correlation (R^2) and the normalised standard deviation (Δq(%) [16,19].

Activation energy (Ea) dependency on rate constant was determined by using the Arrhenius equation (lnk=lnA-Ea/RT) based on the pseudo 1st order and pseudo 2nd order models. Moreover, the Dubinin–Radushkevich (D-R) model was used to calculate the characteristic energy (E). The linear form of the equation is expressed as: $\ln V = \ln V_0 - (RT/\beta E)^2 \ln^2 (P_0/P)$, where V is the volume of adsorbed gas (cm^3/g) given in absolute temperature (T) and relative pressure (P/P_0), V_0 is the microporous volume (cm^3/g), R is the gas constant, β is the

affinity coefficient (0.35 for CO_2) (Guillot & Stoeckli, 2001), and E (kJ/mol) is the characteristic energy for the interaction between the adsorbate and the surface. According to the above equation, the plot of ln (V) against (ln2 (P_0/P)) is a straight line having an intercept with the y-axis equal to the total micropore volume V_0 and the slope equal to the characteristic energy E [20].

2.5. Fixed-bed reactor

Li-LSX zeolite CO_2 capture capacity was also tested at atmospheric pressure at a larger scale in a fixed-bed reactor, in which the zeolite amount was increased by 200 times with respect to that employed in the TGA. It consisted on a downdraft stainless steel fixed-bed reactor (i.d 16 mm and 240 mm length) for testing the same zeolite but at different reactor configuration and in a larger scale. Temperature was controlled using a K-type thermocouple inserted in the zeolite bed. In this case, the experimental procedure was slightly different, since there was not a sample weight change recorded during the adsorption/desorption stages. Instead, the gas composition of the exhaust gas was continuously monitored by a mass spectrometer, MS (MKS Cirrus II). Therefore, for the adsorption tests, 6 g of Li-LSX zeolite were placed in the fixed-bed reactor and tested passing through downdraft the gas stream. In this way, the CO_2 residence time through the sorbent bed was estimated to be around 30 s. Before the adsorption stage, any CO_2, H_2O or impurity was desorbed from the zeolite sample through a pre-desorption step, in which the sample was heated up to 300ºC under 200 ml min^{-1} He flow rate and kept until the CO_2 and H_2O signals from the MS was almost negligible. After that, the reactor was cooled down to the reaction temperature in the same atmosphere. Once the adsorption temperature become stable at 60ºC, the gas stream was switched to a mixture containing 14 vol% CO_2 (in N_2 balance) at a total flow rate of 115 ml min^{-1}, which was held for 40 min to get a steady plateau in the CO_2 MS signal at the reactor outlet once the zeolite

become saturated. After that, the desorption step was performed at 300ºC in 200 ml min^{-1} He. On the other hand, the effect of the presence of small amounts of water was also investigated repeating the same experimental procedure but bubbling the gas stream of 115 ml min^{-1} (14 vol% CO_2 in N_2 balance) through a Drechsel bottle with a sintered head containing water at 20ºC, which resulted in 1.54 vol% H_2O in the gas stream. Then, the CO_2 uptake was calculated based on the difference between the CO_2 breakthrough curve area during the adsorption stage and that obtained for a blank test performed in the same conditions with empty reactor. Breakthrough experiments were carried out in duplicates with errors assessed to be lower than 5%. Since the initial weight loss could not be measured during the experiments performed in the fixed-bed, the corresponding weight loss at 300°C (24 wt%) was taken from the TGA experiment.

To estimate the heat required to desorb the CO_2, the temperature variations related to the amount of gas adsorbed per unit mass of Li-LSX zeolite was calculated in relation to the weight of the sorbent and its adsorption capacity. This temperature was then used to calculate the heat required to desorb the CO_2 (at 300ºC), as previously done by Chen et al. [11]. Q (m*Cp*dT) was calculated considering the Cp of 13X (0.91 kJ/kgK) [21]. The resulting Q (0.33 MJ/kg sorbent) was then normalised to the working capacity of CO_2 captured by 1 kg sorbent at the studied condition.

3. Results and discussion

3.1. CO_2 adsorption capacity and rate using TGA

The effect of the CO_2 concentration (or partial pressure) is an important factor for the adsorption process. Fig. 1 shows a linear relationship ($R^2 > 0.99$) between the CO_2 uptake capacity and the CO_2 concentration in the gas stream. Prior to the adsorption, a calcination step in presence of Helium was carried out at 550ºC for 15 min. It can be observed an

important difference in the adsorption capacity depending on the CO_2 concentration, with capacity increasing from 1.7 mmolCO_2 g^{-1} (14 vol%CO_2 – 5 ml/min) to 4.3 mmolCO_2 g^{-1} (100 vol% CO_2) at the studied conditions.

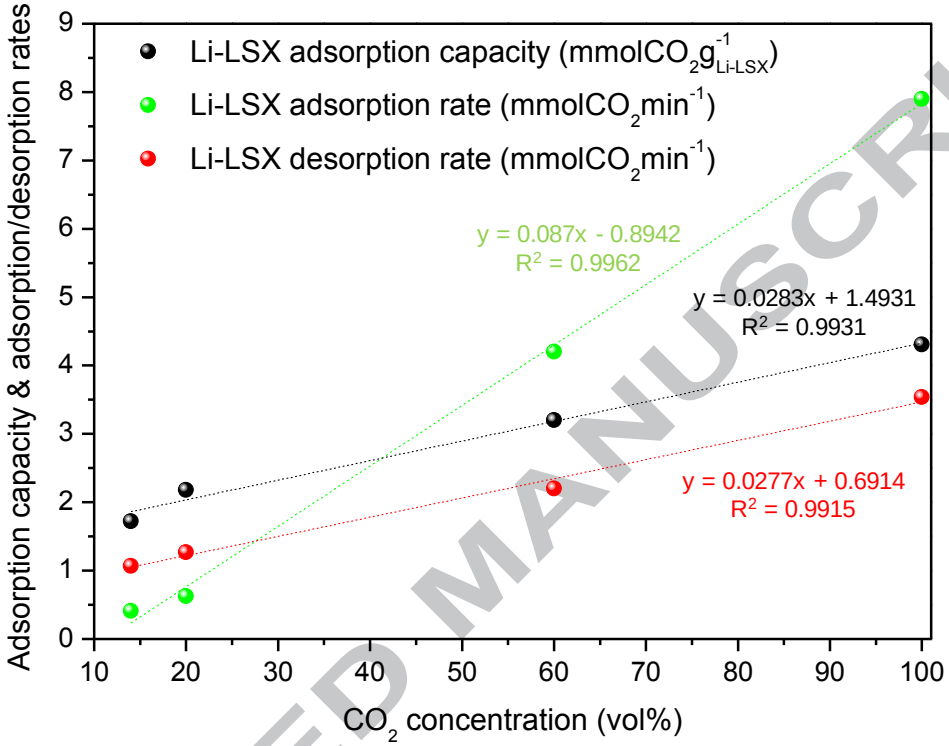

Fig. 1. Effect of CO_2 concentration on the CO_2 uptake capacity and adsorption/desorption rates at 60ºC. Gas stream was balanced with Helium.

To evaluate the stability of Li-LSX under a number of cycles and also to evaluate the adsorption and desorption rates, Fig. 2 shows the CO_2 adsorption/desorption curves of Li-LSX zeolite at 60ºC in presence of 14, 20 and 100 vol% CO_2.

This figure suggests stability under the tested conditions and also indicates a significant variance in the slope of the curves, which reflects also a difference in the adsorption kinetics directly related to the CO_2 partial pressure. This is confirmed by the increase of the CO_2 adsorption rate (See **Fig.** Fig. 2 and Fig. S1 for raw data) from 0.41 mmolCO_2 min^{-1} (14 vol% CO_2) to 0.62 mmolCO_2 min^{-1} (20 vol%CO_2) and ~ 8 mmolCO_2 min^{-1} in presence of 100 vol% CO_2. A similar linear trend was observed for the desorption rate, which increased from 1 mmolCO_2 min^{-1} (14 vol% CO_2) to 3.54 mmolCO_2 min^{-1} (100 vol% CO_2).

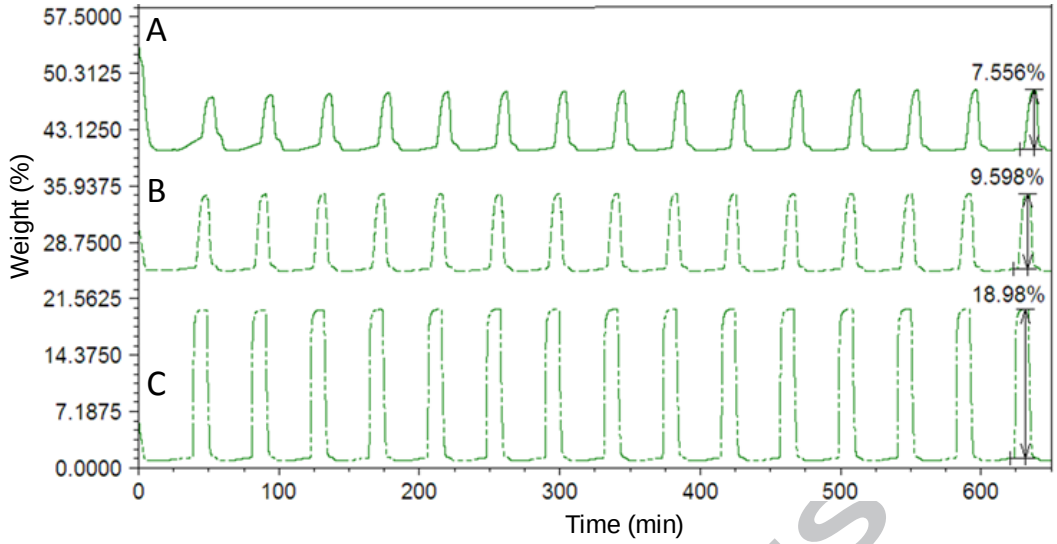

Fig. 2. 15 adsorption/desorption cycles of CO_2 at 60°C in presence of (a) 14, (b) 20 and (c) 100 vol% CO_2. CO_2 flow rate was kept constant at 5 ml min^{-1} and balance with Helium to obtain the desired CO_2 concentrations. Initial calcination at 110ºC (15 min), adsorption at 60ºC and desorption at 420ºC (10 min).

The effect of the adsorption temperature is also a key factor in this process and therefore. Fig. 3 (A and B) shows the combined effect of CO_2 concentration (14 or 100 vol%) and temperature (from 40 to 150ºC) on the adsorption capacity (A) and rates (B) of Li-LSX zeolite. The uptake capacity decreased linearly with adsorption temperature, regardless the CO_2 concentration in the flue gas. The adsorption rates followed the same pattern as for the adsorption capacity (Fig. 3 B), i.e. it decreased linearly with adsorption temperature.

The TGA and DTG profiles of the CO_2 adsorption at the different temperatures is also shown in Fig. S2, where it can be appreciated the reverse proportionality between temperature and CO_2 uptake capacity and adsorption rates. From the desorption curves (Fig. S3), it can be depicted that 60°C was the best temperature in terms of desorption rate and CO_2 adsorption capacity. Despite physisorption at the same temperature of the adsorption (40°C and 60°C) has similar rates (5.3 vs 5.1 wt% min^{-1}), the CO_2 desorbed at 60°C represented 66% of the total CO_2 previously adsorbed, while the percentage dropped to only 47% at 40°C. For a complete desorption, the temperature had to be increased to ~400°C. Higher temperature than

60°C resulted in too low CO_2 uptake capacity to be considered. Therefore, 60°C was selected for the fixed bed experiments. As suggested by Figs. 1-3, the CO_2 adsorption capacity increases with the increasing CO_2 partial pressure, as a result of the facilitated CO_2 diffusion processes. Another interesting information that can be depicted comparing Figs 1 and 3, is the fact that different initial calcination temperatures led to different CO_2 uptake capacities. Therefore, this was further investigated in Section 3.2.

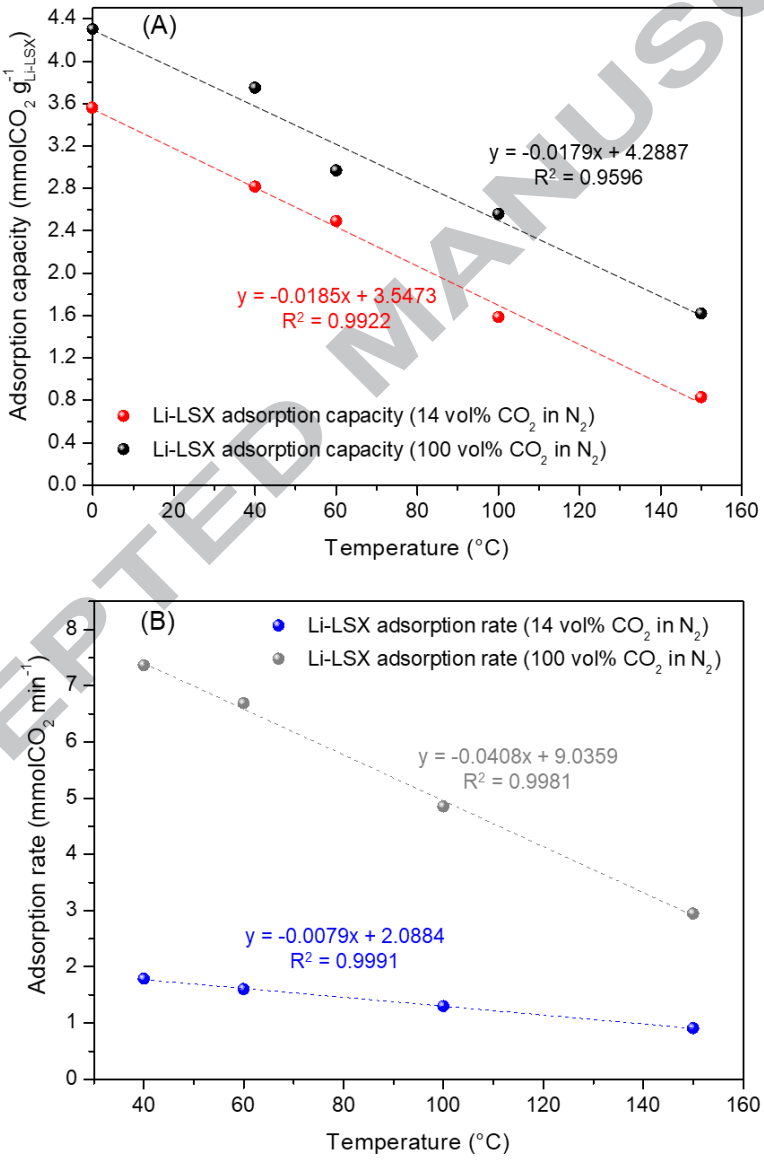

Fig. 3. CO_2 adsorption capacity (A) and adsorption rate (B) of Li-LSX in TGA as a function of adsorption temperature (40 – 150 °C). Gas stream: 14 and 100 vol% CO_2 (in N_2 balance).

A number of models were used to analyse the kinetics of CO_2 adsorption on LiLSX zeolite at different temperatures and under different CO_2 concentrations. The kinetic parameters together to two error functions are reported in Tables 1 and 2. If both errors functions are considered, the kinetic models are found to be suitable for fitting the adsorption kinetic data in the following order: Avrami > Elovich > pseudo 1st order > pseudo 2nd order > intra-particle diffusion kinetic model. Therefore, the Avrami equation, which can account for complex reaction pathways seems the most accurate approach for describing the CO_2 adsorption kinetics on Li-LSX zeolite. The values of the kinetic parameters reported in Table 1 indicate that the adsorption rate constant (K_a) increases with increasing CO_2 concentration. The value of the Avrami exponent, n_A, which is a fractionary number that reflects mechanism changes during the adsorption process, increases when the CO_2 concentration is increased from 14 vol% to 100 vol%, at the CO_2 adsorption has more contact time dependency at the higher concentration. Therefore, as indicated by the kinetics analysis, the CO_2 concentration significantly influenced the adsorption kinetics of Li-LSX zeolite, being 5-fold faster in case of 100 vol%CO_2 in comparison with that of 14 vol% CO_2 as shown in Fig. 3 (B).

Also, n_a between 1.47-1.7 indicates the co-existence of different adsorption mechanisms [19]. The parameters obtained by the Elovich model are α and ß, where α is the initial adsorption rate (mg g-1 min) and β is related to the extent of surface coverage and the activation energy for chemisorption (g mg-1) [17]. α was found to increase according to the increase of CO_2 concentration.

Table 1. Parameters and correlation coefficients obtained from the analysis of CO_2 adsorption kinetics by different equations. CO_2 concentration:100 vol%.

Model	Parameter	40°C	100°C	150°C
1st order pseudo-homog.	**K_1 (1/sec)**	5.30E-02	5.76E-02	4.15E-02
	R^2	0.995	0.960	0.998
	Qe calc.	233.9	152.1	87.3
	$\Delta q_{e\,(\%)}$	17.0	10.5	8.7
2nd order pseudo-	**K_2 (g/mg sec)**	1.92E-06	6.51E-06	1.39E-05

homog.				
	R^2	0.944	0.999	0.993
	Qe calc.	285.7	126.6	106.4
	Δq_e (%)	29.9	4.9	19.5
Elovich	**α (mg/(gmin)**	11.363	8.743	4.809
	ß (g/mg)	0.014	0.020	0.035
	R^2	0.986	0.958	0.997
	Qe calc.	143.1	103.6	74.0
	Δq_e (%)	5.4	3.4	1.1
Intra particle diffusion	**k_1 (mg/g $sec^{0.5}$)**	33.188	9.913	12.737
	C (mg/g)	72.477	42.73	24.99
	R^2	0.981	0.991	0.971
	Qe calc.	295.1	109.2	110.4
	Δq_e (%)	32.2	18.8	21.8
Avrami	**k_{AV} (sec^{-1})**	3.60E-02	3.99E-02	3.35E-02
	n_{AV}	1.700	1.596	1.501
	R^2	0.986	0.959	0.976
	Qe calc.	117.3	114.3	74.2
	Δq_e (%)	0.6	0.5	1.2
Boyd	**Di (m^2/sec)**	1.59E-10	1.84E-10	1.18E-10
	R^2	0.965	0.964	0.985

Table 2. Parameters and correlation coefficients obtained from the analysis of CO_2 adsorption kinetics by different equations. CO_2 concentration:14 vol%.

Model	Parameter	40°C	60°C	100°C
1st order pseudo-homogeneous	**K_1 (1/sec)**	1.20E-02	1.34E-02	1.66E-02
	R^2	0.990	0.987	0.994
	Qe calc.	158.3	148.0	100.0
	Δq_e (%)	15.9	13.8	21.0
2nd order pseudo-homogeneous	**K_2 (g/mg sec)**	1.59E-05	1.56E-05	1.12E-04
	R^2	0.902	0.749	0.975
	Qe calc.	256.4	312.5	108.7
	Δq_e (%)	51.0	90.7	27.4
Elovich	**α (mg/(gmin)**	2.070	1.574	1.264
	ß (g/mg)	0.020	0.023	0.033
	R^2	0.973	0.978	0.986
	Qe calc.	125.4	104.7	76.5
	Δq_e (%)	4.1	2.8	6.5
Intra particle diffusion	**k_1 (mg/g $sec^{0.5}$)**	10.847	9.913	6.273
	C (mg/g)	43.280	42.730	22.920

	R^2	0.981	0.991	0.971
	Qe calc.	200.5	186.4	113.8
	$\Delta q_{e\ (\%)}$	31.0	36.8	29.6
Avrami	k_{AV} (sec^{-1})	8.90E-03	8.54E-03	1.04E-02
	n_{AV}	1.468	1.544	1.673
	R^2	0.996	0.997	0.994
	Qe calc.	125.5	101.3	66
	$\Delta q_{e\ (\%)}$	9.7	1.8	0.6
Boyd	Di (m^2/sec)	1.17E-10	1.27E-10	1.08E-10
	R^2	0.836	0.789	0.920

From the linear plots of the kinetic models depicted in Figures S4 and S5, despite pseudo 1st and pseudo 2nd kinetic models were not the best in fitting the whole experimental data, the first order pseudo kinetic model had a very good fitting in the initial part of the adsorption process, while the second order pseudo kinetic model fitted very well the second part of the adsorption curve, suggesting that physisorption is the dominant mechanism far from adsorption equilibrium. As the Avrami model, the latest also suggests that the adsorption process over Li-LSX is a complex phenomenon. Songolzadeh et al. (2015) described a similar behaviour for the CO_2 adsorption over 13X zeolite [22]. The activation energy (E_a) was calculated by the Arrhenius equation using the K_1 rate constant, resulting in 5.30 kJ/mol and 2.09 kJ/mol for increasing CO_2 concentration from 14 vol% to 100 vol%, indicating that high CO_2 partial pressure facilitated CO_2 adsorption. These values are comparable to those reported for TRI-PE-MCM-41 (1.38 kJ/mol for CO_2 adsorption at 5% concentration) and lower than those obtained using MgAl N1(11.08 kJ/mol) [23-24]. The Adsorption energy (E) obtained from Dubinin–Radushkevich (D-R) isotherm (Fig. S6) was 3.62 kJ/mol corroborating that the uptake of CO_2 onto LiLSX was by physisorption, as indicated by the Ea from the Arrhenius equation.

Regarding the mechanism of CO_2 adsorption, the intra-particle diffusion kinetic model, plotting (qt) vs (t^0.5) did not result in a straight line passing through the origin, indicating that the rate controlling step was not solely intraparticle diffusion and more kinetics stages

were present. The Boyd's film diffusion model was also applied to determine the actual rate controlling step. If a linear function passing through the origin is obtained plotting (Bt) vs (t), the rate of mass transfer is controlled by pore-diffusion, otherwise, as found for LiLSX zeolite, if the function is not linear or linear but not passing through the origin, the CO_2 adsorption rate is controlled by film-diffusion, which is therefore the main resistance to mass transfer [15].

Since most of previous studies report CO_2 uptake for zeolites at temperatures close to 0 °C, the adsorption capacity of Li-LSX-zeolite at 0°C was linearly extrapolated from the results in Fig. 3 (A) for comparison purpose. At the studied conditions, the adsorption capacity at 0 °C was determined to be 4.31 mmol $g_{Li\text{-}LSX}^{-1}$ in the case of pure CO_2 gas stream. To verify the accuracy of the extrapolation, a BET test at 0°C (water-ice bath) instead of -278°C (liquid Nitrogen) was run using CO_2 instead of N_2. The test resulted in a maximum CO_2 capacity (Qm) of 4.21 mmol/g, which confirmed the liner trend (Table S1). Thus, it seems evident that CO_2 concentration, and therefore CO_2 partial pressure, clearly affects the capture capacity of Li-LSX zeolite, decreasing when partial pressure decreases, showing fairly parallel trends when they are plotted versus adsorption temperature.

The effect of temperature in the sorption enhanced water gas shift and biomass reforming processes range (180-250ºC) on the CO_2 adsorption capacity of a higher concentrated exhaust gas (25-32 vol% CO_2) was also examined. Hydrotalcites, which represent the sorbents state of the art for pre-combustion application at intermediate temperatures, have demonstrated to have capacity of 0.5 – 1.25 mmolCO_2 g^{-1} with a 100vol% CO_2 gas at 1 bar and temperature ranging 200 – 400ºC [8,25-26]. In this work, the best performance of Li-LSX in terms of capture capacity of 0.88 mmolCO_2 g^{-1} was obtained at 32 vol% CO_2 and at 180ºC. This value was just below the 1.03 mmolCO_2 g^{-1} obtained with the organo-layered double hydroxides (LDHs) by Wang et al. at 400ºC and 1 bar (CO_2 partial pressure of 0.2 bar); but significantly

higher than that obtained with traditional pre-combustion adsorbents (0.5 mmolCO_2 g^{-1}) reported in the literature [26] suggesting a potential application of Li-LSX at temperature suitable for pre-combustion processes. However, to evaluate the current real potential of Li-LXS zeolite under pre-combustion conditions, high pressure (10-25 bar), real syngas and temperatures below 40°C (as the current acid gas removal processes operate at such low temperatures) should be assessed.

3.2. Effect of the calcination temperature on the CO_2 adsorption

The effect of three different calcination temperatures (150, 300 and 550ºC) on the CO_2 adsorption process was investigated at 60ºC by TGA using 14 vol%CO_2 (balanced with N_2) and Li-LSX in pellets. The breakthrough curves are shown in Fig. S7, where it can be clearly seen that the higher the calcination temperature, the larger the weight loss in the beginning of the experiment during the calcination step (19.7 wt% (150ºC) < 24 wt% (300ºC) < 25.1 wt% (550ºC); but also, the greater is the adsorption capacity as shows Fig. 4. This is especially true when the temperature is risen from 150 to 300ºC, (increasing from 0.45 to 1.46 mmolCO_2 g^{-1}). Then, at higher calcination temperature (550ºC) the adsorption capacity growth is smoothed up to 1.9 mmolCO_2 g^{-1}. The rate of adsorption also increases with the calcination temperature passing from 0.15 mmolCO_2 min^{-1} (150ºC) to 0.54 and 0.67 mmolCO_2 min^{-1} after calcination at 300 and 550ºC, respectively. This suggests that a calcination of at least 300ºC is beneficial to the CO_2 adsorption on Li-LSX, using a TGA set-up. Fan et al (2015) showed that calcination of Li-LSX zeolite up to 226 °C released physisorbed water, while the release of chemisorbed water required temperatures between 226 and 427 °C [27]. But also, in Fig. S7 is observed that not all the CO_2 adsorbed on the Li-LSX-zeolite is desorbed at 60ºC, suggesting that the working capacity of the material (in presence of N_2) if desorption is carried out at the same temperature of the adsorption are 71.7 wt% (of the maximum adsorption), 74.9 wt% and 78.9 wt% after calcination at 150, 300 and 550ºC, respectively.

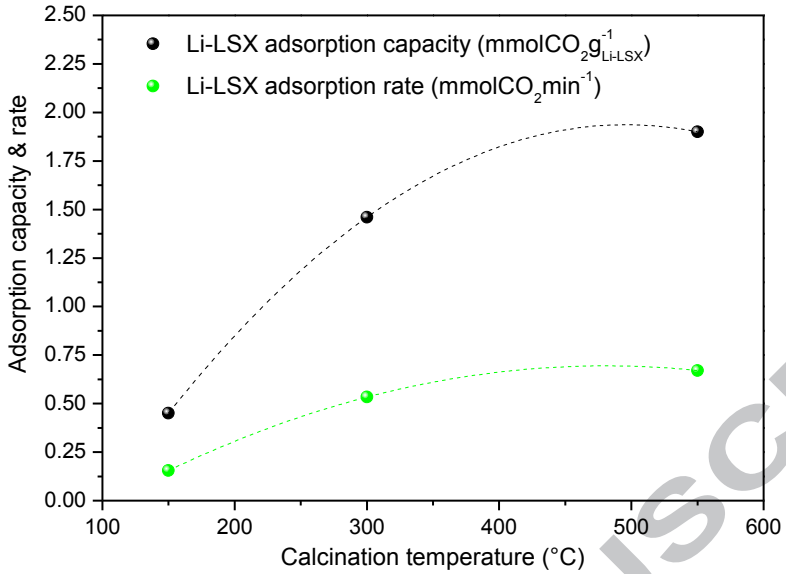

Fig. *4*. Calcination Temperature vs. Adsorption capacity and rate, and versus gases desorbed during calcination. Sample in pellet form was used for these tests. Initial desorption at 550°C for 60 min.

To investigate the reasons behind the enhanced CO_2 uptake and adsorption rate after calcination at high temperature, a series of analysis were carried out, including XRD, BET, basicity tests and MS. As shown in Fig. 5, the characteristic peaks related to the FAU structure indexed at (111), (220), (331), (533), (553) and (715) were clearly observed on the Li-LSX patterns up to calcination at 550ºC, suggesting that Li-LSX retains its framework structure up to that temperature. This is in agreement with previous work, where 700ºC was found to be the thermal stability limit of Li-LSX [27]. The XRD patterns obtained at the different calcination temperatures did not show particular differences, which were limited to the increase of the intensity and a shift of the peaks at lower 2θ degree according to the increase of the calcination temperature, which can be linked to increased crystallinity. To confirm that, the variance of relative crystallinity as a function of the calcination temperature is presented in Fig. S8, where there is an increase of the crystallinity index from 1 (raw Li-LSX) to 1.6/1.7 by annealing, due to smaller grains agglomeration resulting in bigger grains, which increase the crystalline quality and grain size. Similarly, in one of our previous works

employing Li-LSX zeolite, XRD suggested minor changes in the Li-LSX-zeolite framework when calcined up to 300ºC [28].

Possible surface modifications taking place by calcination were evaluated by analysis the BET surface, micropore surface and volume and isotherm of LiLSX under different calcination temperatures. The isotherms (Fig S9) obtained after different calcination temperatures resulted of Type-I, typical of microporous material that shows a rapid increase in the adsorption uptake in the low relative pressure range (P/Po<0.1) with increase in the pressure or concentration, followed by the gentle gradient in the uptake until the saturation pressure. Table 3 indicates that the microporous volume and surface decrease by increasing the calcination temperature due to cell volume contraction by dehydration [27], while inversely, the external surface increases. The DFT curves (Fig. S10) indicate an increase of mesopores with diameter between 2-3 and 15-20 nm. A similar micropore volume and external surface were obtained at 300 and 550°C. Despite the decrease of the micropore volume at high calcination temperature, the external surface increased by 70-85%, which could be linked to the enhanced adsorption rates, since the CO_2 adsorption limiting step was identified in the diffusion of the CO_2 from the bulk phase (boundary layer) to the external surface of the sorbent (film diffusion) by the kinetic analysis (See Section 3.1).

Table 3. Surface analysis of LiLSX after calcination at different temperatures.

	Calcination temperature (°C)		
	Raw*	300*	550*
BET (m^2/g)	660	400	436
Micropores (m^2/g)	620	327	359
Micropore volume (cm^3/g)	0.31	0.18	0.18
Externa surface (m^2/g)	42	71	78

* BET degassing at 200°C

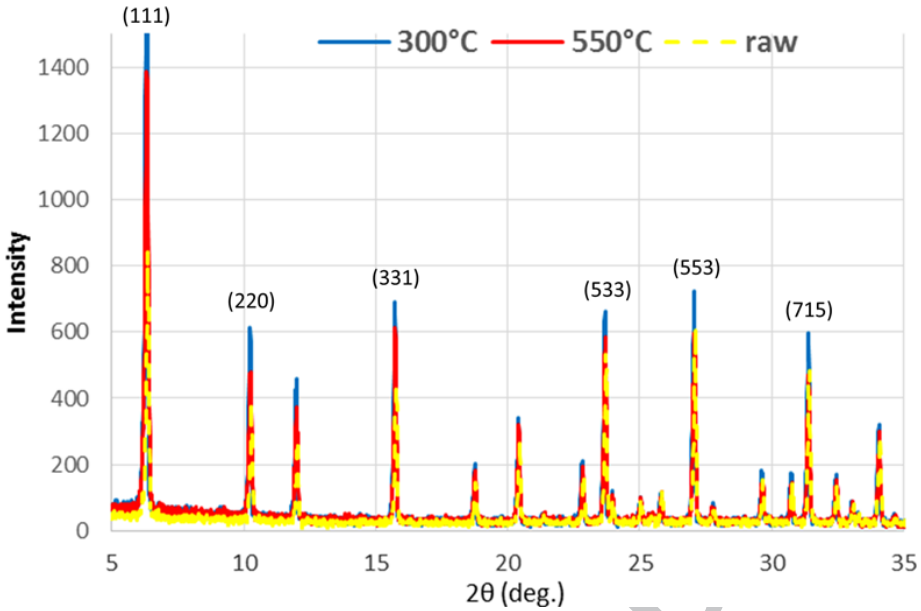

Fig. *5*. XRD patterns of the raw Li-LSX zeolite and those corresponding to the same zeolite calcined at different temperatures and tested for CO_2 capture at 60 °C.

Similarly, Lu et al. found that the HZSM-5 BET surface area and acidity decrease with increasing calcination temperature from 500 to 800 °C, but this was not related to changes in the frame structure [29]. To confirm any changes in the Li-LSX basicity after calcination at different temperature, a series of CO_2-TPD tests were carried out using the Li-LSX zeolites calcined at the three different temperatures. The CO_2 released at 60°C (peak 1) can be ascribed to physisorbed CO_2, which is in agreement with previous work showing water release at surface or inside microporous channels of the LSX skeleton at SI site [30]. Fig. 6 a, b suggests also that chemically bonded CO_2 is released when the zeolite is heated at temperature up to 300ºC, which well corresponds to the loss of chemisorbed water from SII site in LSX supercage as previously reported [15,27]. Finally, the third high temperature weight loss (up to 530ºC) for the Li-LSX calcined at 550ºC (Fig. 6 a) was ascribed to desorption of CO_2 from SIII site present in supercage. Furthermore, these observations suggest that CO_2 desorption process in Li-LSX zeolite took place first from SI at the surface followed by the SII and SIII sites present in the supercage, as denoted in previous studies for

the desorption of water [30-31]. The Li-LSX zeolite basicity increased in the following order: 0.031 mmolCO_2/g (60°C) < 0.31 mmolCO_2/g (300°C) < 1.22 mmolCO_2/g (550°C).

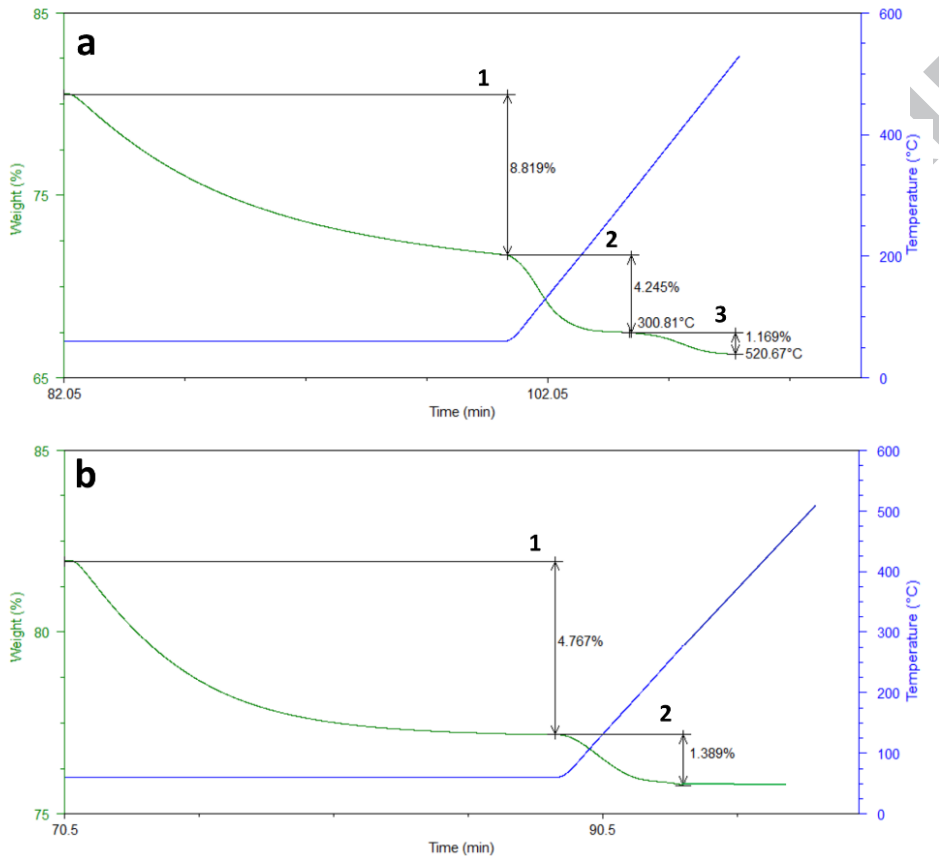

Fig. 6. Li-LSX zeolite CO_2-TPD tests at different calcination temperatures: a) 550ºC; b) 300ºC.

To compare the water release trend during the calcination at 300ºC with that shown in previous work [31] , the MS of the gases evolved during the calcination are reported in Fig. 7, where can be seen that with the raise of the temperature, physically adsorbed water, CO_2 and N_2 are released first from SI sites in the micro-channels. Then, when the temperature is close to 300ºC, chemically bonded CO_2 and water were released from the Li-LSX zeolite SII and SIII sites in the supercage. Therefore, the increased CO_2 adsorption rates of the zeolite after being calcined at 300ºC and 550ºC in the TGA, can be mainly linked to an enhanced removal of adsorbed water/CO_2/N_2, which increased the Li-LSX basicity due to Li ions freed from

bonded water in the pores and reduced mass transfer limitation due to pore opening modifications (See Table 3).

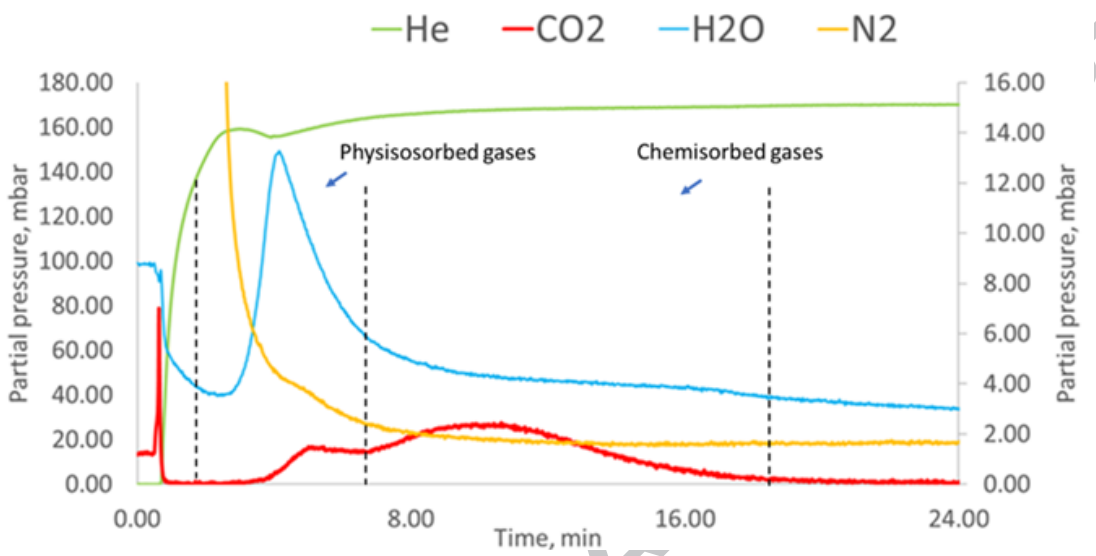

Fig. 7. Mass Spectrum of gases during the calcination at 300°C carried out in Helium atmosphere. He partial pressure scales to the left Y-axis, all other gases to the right Y-axis.

3.3. Cyclic adsorption-desorption performance (TGA)

Another decisive parameter for the selection of a proper adsorbent in the scaling up the CO_2 capture process is the adsorbent performance over multiple-cycles operation. Figure 2 already showed that the adsorption/desorption of CO_2 on Li-LSX zeolite was stable in presence of CO_2, but in a real scenario, CO_2 will be diluted in N_2. Therefore, an experiment that involved 85 adsorption/desorption cycles over more than 35 hours period was carried out in the TGA with Li-LSX zeolite with a gas stream containing 14 vol% CO_2 (in N_2 balance), and the resulting performance is presented in Fig. 8. It is clear from the graph that there are not major variations in the adsorption capacity even after 85 cycles and 35 hours. From the figure, it appears that a cyclic somehow steady state was reached after first 5 cycles. The CO_2 working capacities ($mmolCO_2\ g^{-1}$) and the adsorption/desorption rates ($mmolCO_2\ min^{-1}$) of each cycle are reported in Fig. S11. The adsorption and desorption rates were in average 0.97 and 1.1

mmolCO_2 min^{-1}, while the working capacity was ~2.45 mmolCO_2 g^{-1}. In future work, it would be interesting to see how the presence of other contaminants and in particular water from the flue gas would affect the results in Fig. 8. Previous works found out that the Li-LSX zeolite CO_2 adsorption capacity from air stream decreased from 0.82 to 0.01 mmolCO_2 g^{-1} when a wet air stream (80% relative humidity) containing 395 ppm of CO_2 was used at 25 °C [13]. However, this extreme moisture content is not typical of coal or industrial CO_2 emitters.

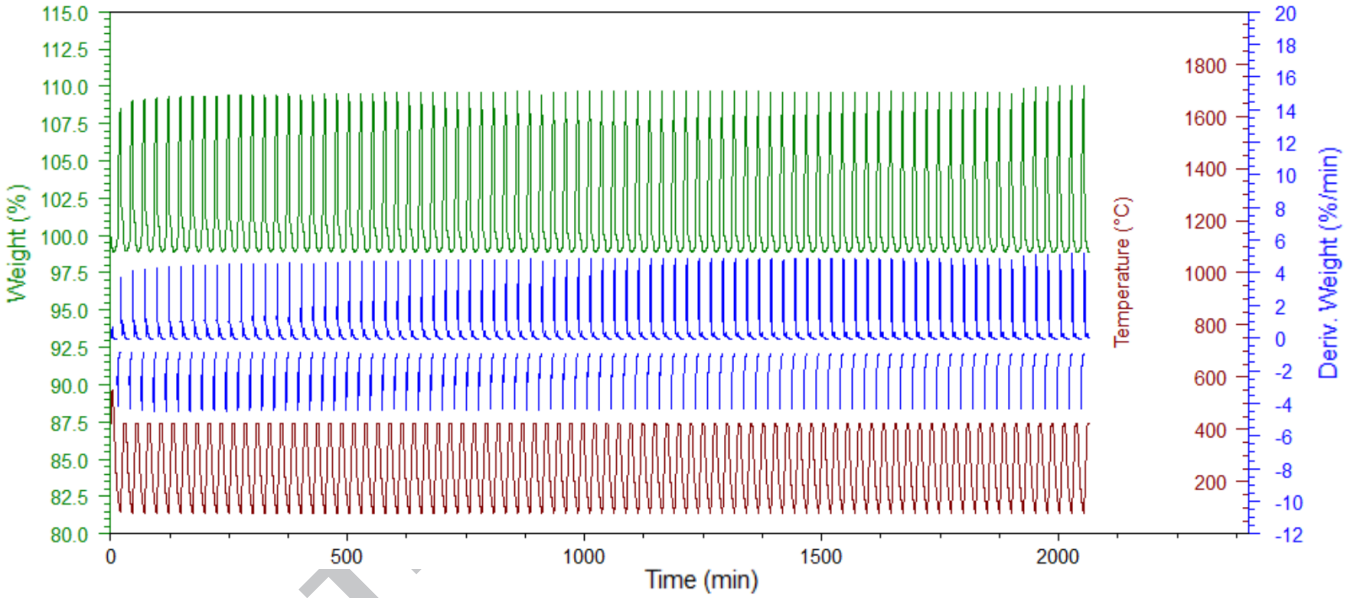

Fig. 8. Performance of Li-LSX zeolite over 85 adsorption/desorption cycles at 60 °C. Gas stream: 16 ml min^{-1} of 14 vol% CO_2 in N_2 balance).

3.4. Fixed-bed experiments

Fig. 9 (A) shows the comparison of the CO_2 breakthrough curves of Li-LSX zeolite as relative concentration (expressed as C/C_0) between the adsorption tests performed in dry and wet conditions. A number of minutes were required to stabilise the partial pressure in presence of moisture, as denoted by the "CO_2 blank-wet gas" being higher than 1 (C/C0) in the first minutes. It can be observed that the breakthrough curve was somehow delayed when CO_2 gas stream contained little amount of moisture (1.54 vol%). Thus, CO_2 was fully adsorbed in the Li-LSX zeolite for as long as 24 and 22 minutes for the wet and dry gas streams, respectively.

The CO_2 physisorption on the Li-LSX zeolite is evidently an exothermic reaction both, in dry or wet conditions, from what can be observed in Fig. 9 (B), which plots the temperature profiles of the Li-LSX zeolite during the adsorption step. There was an increase in the temperature from 62ºC to a maximum of 84 and 86ºC, for tests performed in dry and wet conditions, respectively. In both cases, the sample temperature decreased to the set value once the sample became saturated and CO_2 started to be present at the outer gas. This can be explained by Van der Waals reversible interactions between CO_2/N_2 and Li-LSX-zeolite, with the conversion of the kinetic energy of the gaseous species into heat [11]. This also implicates that since the process is exothermic, the amount of CO_2 adsorbed decreases with increasing temperature (See Fig. 3 A), due to decrease in adsorbent density during the adsorbate-adsorbent interactions. Since some of the heat generated is absorbed by the adsorbent, this led to a decrease of the CO_2 adsorption with increasing temperature [15].

The temperature variations related to the amount of gas adsorbed per unit mass of Li-LSX zeolite was used to calculate the heat required to desorb the CO_2 (by temperature swing at 300ºC), which resulted in 2.86 MJ/kgCO_2 in dry conditions, when normalised to the working capacity (1.86 MJ/kgCO_2 if based on the fix-bed experiments). The normalised value resulted similar to those obtained by Chen et al. [11] in a previous work, using Li-X and LiPdAg-X zeolites respectively, which is well below the energy requirement for regenerating MEA (at 120ºC) (3.2-4.2 MJ/kg_{CO2}) and comparable to that required by the state of the art solvent KS-1^{TM} (2.44 MJ/kgCO_2) developed by Mitsubishi Heavy Industries and used in the Petra Nova post-combustion CO_2 capture plant in US [32]. It has to be considered that the thermal regeneration is not the most energy-efficient way to desorb CO_2 from zeolites. In fact, other work resulted in lower energy penalties for the desorption of CO_2 using Vacuum Swing Adsorption (VSA) (4-step cycle) and zeolite 13X, where the total energy required for achieving 90%CO_2 purity with an P_{In} of 0.16 bar and a P_{Fin} of 0.03 bar, was 0.63 MJ/kg_{CO2}

[33]. This suggests that the use of VSA for the regeneration of Li-LSX at 60°C would result in a substantial decrease of the energy penalty compared to the thermal regeneration used in this work.

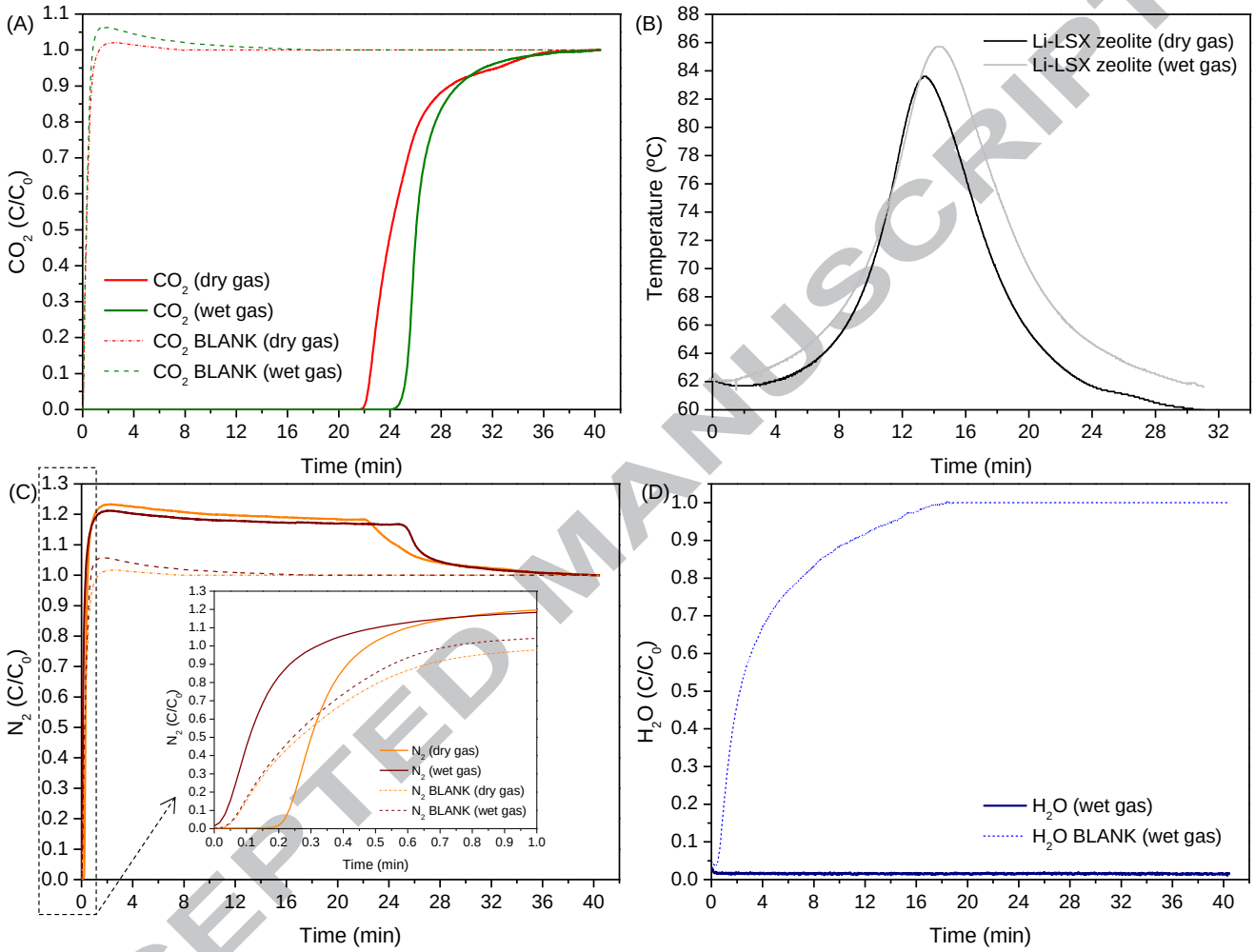

Fig. 9. CO_2 breakthrough curves (A), N_2 (C) and H_2O (D) as relative concentrations (expressed as C/C_0) comparison between the adsorption tests in dry and wet conditions of Li-LSX zeolite at 60 °C. (B): Zeolite temperature profile during the adsorption tests.

Fig. 9 (C) shows the N_2 relative concentration with time on stream for both tests, in dry and wet conditions. What can be observed from this figure is that only in the case of the dry gas stream there was a certain N_2 adsorption on the zeolite, which can be appreciated from the zoom image, where both N_2 curves corresponding to dry conditions, the adsorption and the corresponding blank crosses. The reason of having a drop in the signal (N_2 wet and dry) after 22 min is because the gas signals in Fig. 9 (C) are expressed as relative values with respect to

the gases partial pressures. Therefore, at the beginning, the relative partial pressure value of N_2 is higher than 1 because the CO_2 is being adsorbed, so the N_2 partial pressure is higher than that of the initial N_2-CO_2 mixture, being C/C0 > 1. Then, once the zeolite becomes "suddenly" saturated, the CO_2 partial pressure sharply increases with the corresponding decrease in the N_2 one and therefore, the relative partial pressure goes to 1. On the other hand, there is a clear evidence from Fig. 9 (D) that all the water contained in the gas stream during the experiment carried out at wet conditions was physisorbed on the zeolite. In presence of moisture in the gas, H_2O is also adsorbed since the beginning of the adsorption step and this obstacles the adsorption of N_2 in the beginning of the adsorption test. In both tests, the zeolite was fully desorbed after saturation by means of a desorption step carried out at 300ºC in He flow.

Table 4 summarises the results of the adsorption capacity and selectivity to CO_2 obtained with the Li-LSX zeolite in the fixed-bed during the adsorption tests in dry and wet conditions at 60ºC and different calcination temperatures. Firstly, the zeolite calcination temperature modified its CO_2 adsorption capacity, which was reduced in less than 10 mol% when the sample was calcined at 300ºC, with respect to that calcined at 60°C. This can be explained mostly by the decrease in micro-porosity on the Li-LSX surface when calcined at 300°C, as clearly supported by the surface analysis shown in Table 3. In the same way, its capacity to adsorb N_2 was also diminished with calcination temperature. Then, as a result of that, Li-LSX zeolite presented 1.5 times higher CO_2 selectivity when it was subjected to a calcination process at 300ºC.

It has to point out that the results obtained using the fix-bed are not directly comparable with those obtained using the TGA for a number or reasons such as: (1) different CO_2 and total gas flow rates were used; (2) He was used in the fix-bed desorption stage; (3) different adsorption/desorption times were used. However, an important aspect that can be highlighted

from the indirect comparison of the two set-ups, is that the degassing in the fixed-bed set-up is much more efficient than in the TGA (already at 60°C), since the gas can across almost freely the pellets, while in the TGA, the temperature must be raised to degas the Li-LSX zeolite.

Moreover, as shown in Fig. 9, the presence of a small percentage of moisture in the CO_2 gas stream improved the Li-LSX performance, not only in terms of CO_2 adsorption capacity (7 mol% higher); but also, in terms of selectivity to CO_2, because no N_2 adsorption was observed when the wet gas stream was fed. In this case, the CO_2 could be easily separated during the desorption process from the water by means of the condensation of the latter.

Table 4. CO_2 adsorption and desorption capacity of the zeolite at 60 °C and 14%vol CO_2 (in N_2)

Exp.	Calcination temperature (°C)	GAS	Capacity		Selectivity
			(mmol g^{-1})	(wt%)	
Dry gas	60	CO_2	4.43	19.49	85.7
		N_2	0.318	0.89	
	300	CO_2	4.00	17.60	128.1
		N_2	0.192	0.54	
Wet gas	300	CO_2	4.29	18.89	
		N_2	0.000	0.00	
		H_2O	0.713	1.28	

Therefore, as it has already seen, selectivity to CO_2 over other compounds in the post-combustion (N_2, H_2O, O_2, etc.) gas streams is a key factor for any adsorbent to be viable at commercial scale utilisation and, therefore it needs be significantly high because it will determine the purity of the captured CO_2 stream [8,34].

In this work, we have investigated the CO_2 selectivity of Li-LSX zeolite over N_2 in the fixed-bed reactor as they are the main components of post-combustion flue gas at industrial scale. Therefore, Table 5 summarizes the selectivity to CO_2 of Li-LSX in comparison with other

zeolites, which were benchmarked in previous papers [11,35-37]. In terms of selectivity, Li-LSX zeolite performance resulted even higher than that showed by other zeolites, like Li-ZK5, which has demonstrated to have one of the best performances up to date. These selectivity values were obtained based on experiments that were done at ideal conditions (dry conditions). One of the properties that can affect the CO_2 uptake of the zeolites is their surface area and pores volume, in particular the micropore volume. In a previous work, Li-X and LiPdAg-X zeolites resulted in BET surface area of 560 and 549 $m^2\ g^{-1}$ and a pores volume of 0.30 and 0.29 $cm^3\ g^{-1}$, respectively [11]. The larger micropore volume of the Li-LSX-zeolite could be responsible for the larger CO_2 uptake, as shown in Table 5, while the higher selectivity towards CO_2, when the material is calcined at 300°C, can be linked to the increased basicity of the material and increased presence of "free metal sites" into the pores.

Table 5. Comparison of the CO_2 and N_2 uptakes and the selectivity to CO_2 at 0°C (unless otherwise stated) of the Li-LSX zeolite with respect other zeolites from the literature.

Adsorbent	CO_2 uptake, 0.15 bar (mmolCO_2 g^{-1})	N_2 uptake, 0.85 bar (mmolCO_2 g^{-1})	Selectivity	Pore volume ($cm^3\ g^{-1}$)	V_{mic} ($cm^3\ g^{-1}$)	BET specific surface area ($m^2\ g^{-1}$)	A_{ext} ($m^2\ g^{-1}$)	Pore size (Å)	Si/Al ratio	Ref.
Li-LSX*	4.21/(4.00**)	0.19**	128.00**	0.32	0.31	662.00	42.00	0.80-1.80	1.00	This work
Li-CHA	4.40	0.53	47.00	0.27	0.27	-	27.00	3.60-3.80	6.00	[35,37]
Li-RHO	4.60	-	-	0.34^^	-	-	-	1.90	3.20	[35,36]
Li-ZK5	3.90	0.23	96.00	-	0.22	-	-	-	5.00	[35]
Ba-CHA	3.00	1.10	15.00	0.27	0.27	-	27.00	3.60-3.80	6.00	[35,37]
LiPdAg-X **,^	1.80	-	-	0.29	-	549.00	-	0.70-0.90	-	[11]
Li-X***,^	1.30	-	-	0.30	-	560.00	-	0.70-0.90	-	[11]
13X**,^	-	-	-	0.27	0.34	537.00	-	0.70-0.90	1.25	[11]

*0.14 bar CO_2 / 0.86 bar N_2; **T: 60 °C.; ***T:25°C; ^ 1.5 bar using 3%CO_2/97%N_2; ^^ pure RHO

3. Conclusions

Li-LSX-zeolite potential as CO_2 sorbent for post-combustion carbon capture systems was evaluated. The TGA tests indicated a linear decrease of the CO_2 adsorption capacity and adsorption rate at the increase of the adsorption temperature, regardless the CO_2 concentration. Calcination at temperatures > 300°C resulted effective in increasing the CO_2 adsorption rates, due to enhanced removal of adsorbed species, pore opening modifications and increased availability of basic site in the micropores.

Among a number of kinetic models, the Avrami equation was the most suitable for fitting the CO_2 adsorption kinetic data, suggesting the coexistence of different adsorption mechanisms. Using the Arrhenius equation, the E_a was found to be 2 and 5 kJ/mol for the 14 vol% and 100 vol% CO_2, respectively, indicating physisorption. The adsorption rate constant (K_{av}) increased with the increasing CO_2 partial pressure, as a result of the facilitated CO_2 diffusion processes. The intra-particle diffusion kinetic model and the Boyd film diffusion model indicated that film diffusion was the rate-limiting step for the CO_2 adsorption.

The fixed-bed breakthrough experiments resulted in a continuous CO_2 adsorption of 24 and 22 minutes for the wet and dry gas streams, respectively, with the physisorption being exothermic. The maximum CO_2 sorption capacity of 4.43 mmol g^{-1} was obtained after an initial calcination at 60°C in presence of 14%CO_2 due to high micropore volume (0.31 cm^3/g), but the best CO_2 selectivity (128.1) was obtained calcining the Li-LSX zeolite at 300°C, which can be linked to enlargement of external surface and large number of basic sites freed during the calcination process..

Presence of water traces (1.53 vol%) also increased the CO_2 capacity from 4.00 to 4.29 mmol g^{-1} after zeolite calcination at 300ºC. The stability of Li-LSX in presence of 14 vol% CO_2 was

shown to be excellent over 85 adsorption/desorption cycles with Li-LSX showing almost no degradation over the 35 hours and a working capacity of 2.45 mmolCO_2/g with adsorption/desorption cycle of 6 and 5 minutes, respectively. The adsorption performance testing showed that Li-LSX has comparable adsorption capacity and rates below 80 °C with most zeolites in literature but one of the highest selectivity to CO_2 (128). This was related to the high surface area (662 m^2 g^{-1} and the high affinity of the Li^+ cations in the zeolite towards CO_2.

The energy required for the endothermic desorption of the CO_2 (2.4-2.8 MJ/kgCO_2) by Thermal Regeneration (TR) at 300°C, resulted comparable to that required for regenerating KS-1^{TM} solvent (2.44 MJ/kgCO_2), while consistent less energy is expected if Vacuum Swing Adsorption (VSA) is used instead of TR, which makes Li-LSX zeolite a promising candidate for post-combustion applications.

Acknowledgements

The authors gratefully acknowledge the EPSRC for financial support (grant no. EP/P018955/1) and the RCCS at Heriot-Watt for TGA access.

References

[1] ESRL, NOAA, trends in Atmospheric Carbon Dioxide, Recent Global CO_2, 2018. https://www.esrl.noaa.gov/gmd/ccgg/trends/global.html, 2018, (accessed 20 August 2018).

[2] L.M. O. D. Bert Metz, H. de Coninck, M. Loos, Special report on carbon dioxide capture and storagee, Cambridge, England, 2005, https://www.ipcc.ch/pdf/special-reports/srccs/srccs_wholereport.pdf (Accessed 12 June 2018).

[3] Y. Wang, L. Zhao, A. Otto, M. Robinius, D. Stolten, A Review of Post-combustion CO_2 Capture Technologies from Coal-fired Power Plants. Energy Procedia 114 (2017) 650–665. doi:10.1016/j.egypro.2017.03.1209.

[4] A.S. Bhown, B.C. Freeman, Analysis and status of post-combustion carbon dioxide capture technologies, Environ. Sci. Technol. 45 (2011) 8624–8632. doi:10.1021/es104291d.

[5] K.A. Fayemiwo, G.T. Vladisavljević, S.A. Nabavi, B. Benyahia, D.P. Hanak, K.N. Loponov, V. Manović, Nitrogen-rich hyper-crosslinked polymers for low-pressure CO_2 capture, Chem. Eng. J. 334 (2018) 2004–2013. doi:10.1016/j.cej.2017.11.106.

[6] R. Ben-Mansour, M.A. Habib, O.E. Bamidele, M. Basha, N.A.A. Qasem, A. Peedikakkal, T. Laoui, M. Ali, Carbon capture by physical adsorption: Materials, experimental investigations and numerical modeling and simulations - A review, Appl. Energy. 161 (2016) 225–255. doi:10.1016/j.apenergy.2015.10.011.

[7] S. Loganathan, A.K. Ghoshal, Amine tethered pore-expanded MCM-41: A promising adsorbent for CO_2 capture, Chem. Eng. J. 308 (2017) 827–839. doi:10.1016/j.cej.2016.09.103.

[8] J. Wang, L. Huang, R. Yang, Z. Zhang, J. Wu, Y. Gao, Q. Wang, D. O'Hare, Z. Zhong, Recent advances in solid sorbents for CO_2 capture and new development trends, Energy Environ. Sci. 7 (2014) 3478–3518. doi:10.1039/C4EE01647E.

[9] M. Mohamedali, H. Ibrahim, A. Henni, Incorporation of acetate-based ionic liquids into a zeolitic imidazolate framework (ZIF-8) as efficient sorbents for carbon dioxide capture, Chem. Eng. J. 334 (2018) 817–828. doi:10.1016/j.cej.2017.10.104.

[10] A.A. Leonova, M.S. Melgunov, Alteration of Adsorption Selectivity of LSX Zeolite in Li+ and H+ forms towards CO_2 and N_2O, Catal. Sustain. Energy. 4 (2017) 31–35.

[11] S.J. Chen, M. Zhu, Y. Fu, Y.X. Huang, Z.C. Tao, W.L. Li, Using 13X, LiX, and LiPdAgX zeolites for CO_2 capture from post-combustion flue gas, Appl. Energy. 191 (2017) 87–98. doi:10.1016/j.apenergy.2017.01.031.

[12] J.C. Knox, D.W. Watson, T.J. Giesy, N. Marshall, S. Flight, Investigation of Desiccants

and CO_2 Sorbents for Exploration Systems 2016-2017, (2017), https://ntrs.nasa.gov/archive/nasa/casi.ntrs.nasa.gov/20170008962.pdf (Access May 2018).

[13] N.R. Stuckert, R.T. Yang, CO_2 capture from the atmosphere and simultaneous concentration using zeolites and amine-grafted SBA-15, Environ. Sci. Technol. 45 (2011) 10257–10264. doi:10.1021/es202647a.

[14] F. Brandani, D.M. Ruthven, The Effect of Water on the Adsorption of CO_2 and C_3H_8 on Type X Zeolites, Ind. Eng. Chem. Res. 43 (2004) 8339–8344. doi:10.1021/ie040183o.

[15] V. K. Singh and E. A. Kumar. Measurement of CO_2 adsorption kinetics on activated carbons suitable for gas storage systems, Greenhouse Gas Sci Technol. 7 (2017) 182–201. doi.org/10.1002/ghg.1641

[16] W. J. Weber WJ and J. C. Morris, Kinetics of adsorption on carbon from solution. J. Sanitary Eng. Div. 89 (1963) 31–59.

[17] F.C. Wu, R.L. Tseng, R.S. Juang, Characteristics of Elovich equation used for the analysis of adsorption kinetics in dye-chitosan systems, Chem. Eng. J. 150 (2009) 366-373. doi.org/10.1016/j.cej.2009.01.014

[18] L. Stevens, K. Williams, W.Y. Han, T. Drage, C. Snape, J. Wood, J. Wang, Preparation and CO_2 adsorption of diamine modified montmorillonite via exfoliation grafting route, Chem. Eng. J. 215–216 (2013) 699–708. doi: 10.1016/j.cej.2012.11.058

[19] N. Álvarez-Gutiérrez, M.V. Gil, , F. Rubiera, C. Pevida, Kinetics of CO_2 adsorption on cherry stone-based carbons in CO_2/CH_4 separations, Chem. Eng. J. 307 (2017) 249–257.

[20] F. Ouadjenia, R. Marouf and J. Schott, Mechanism sorption of carbon dioxide onto dam silt, Cogent Chemistry 3 (2017), 1300974. doi.org/10.1080/23312009.2017.1300974

[21] Y. Hirasawa, W. Urakami, Study on Specific Heat of Water Adsorbed in Zeolite Using

DSC, Int. J. Thermophys 31 (2010) 2004–2009. doi 10.1007/s10765-010-0841-6.

[22] M. Songolzadeh, M. Soleimani, M.T. Ravanchi, Using modified Avrami kinetic and two component isotherm equation for modelling of CO_2/N_2 adsorption over q 13X zeolite bed. J. Nat. Gas Sci. Eng. 27 (2015) 831-841. doi:10.1016/j.jngse.2015.09.029

[23] R. Serna-Guerrero, A. Sayari, Modeling adsorption of CO_2 on amine-functionalized mesoporous silica. 2: Kinetics and breakthrough curves. Chem. Eng. J. 161 (2010) 182-190. doi.org/10.1016/j.cej.2010.04.042

[24] J. W. Wang, L. A. Stevens, T. C. Drage, J. Wood, Preparation and CO_2 adsorption of amine modified Mg-Al LDH via exfoliation route. Chem. Eng. Sci. 68 (2012) 424-431. doi.org/10.1016/j.ces.2011.09.052

[25] D. Cebrucean, V. Cebrucean, I. Ionel, CO_2 capture and storage from fossil fuel power plants, in: Energy Procedia 63 (2014) 18–26. doi:10.1016/j.egypro.2014.11.003.

[26] L. Hauchhum, P. Mahanta, Carbon dioxide adsorption on zeolites and activated carbon by pressure swing adsorption in a fixed bed, Int. J. Energy Environ. Eng. 5 (2014) 349–356. doi:10.1007/s40095-014-0131-3.

[27] M. Fan, J. Sun, S. Bai, H. Panezai, Size effects of extraframework monovalent cations on the thermal stability and nitrogen adsorption of LSX zeolite, Microporous Mesoporous Mater. 202 (2015) 44–49. doi:10.1016/j.micromeso.2014.09.011.

[28] N.A. Abd Rahman, J. Fermoso, A. Sanna, Effect of Li-LSX-zeolite on the in-situ catalytic deoxygenation and denitrogenation of Isochrysis sp. microalgae pyrolysis vapours, Fuel Process. Technol. 173 (2018). 253-261. doi.org/10.1016/j.fuproc.2018.01.020

[29] J. Lu, Z. Zhao, C. Xu, A. Duan, P. Zhang, Effects of calcination temperature on the acidity and catalytic performances of HZSM-5 zeolite catalysts for the catalytic cracking of n-butane, J. Nat. Gas Chem. 14 (2005) 213–220.

doi:10.1016/j.ijfoodmicro.2004.12.017.

[30] M. Fan, H. Panezai, J. Sun, S. Bai, X. Wu, Thermal and kinetic performance of water desorption for N_2 adsorption in Li-LSX zeolite, J. Phys. Chem. C. 118 (2014) 23761–23767. doi:10.1021/jp5068236.

[31] H. Panezai, M. Fan, J. Sun, S. Bai, X. Wu, Influence of Ca^{2+} or Na^{+} extraframework cations on the thermal dehydration and related kinetic performance of LSX zeolite, J. Phys. Chem. Solids. 99 (2016) 1–10. doi:10.1016/j.jpcs.2016.07.025.

[32] M. Iijima, T. Nagayasu, T. Kamijyo, S. Nakatan, MHI 's Energy Efficient Flue Gas CO_2 Capture Technology and Large Scale CCS Demonstration Test at Coal-fired Power Plants in USA, Mitsubishi Heacy Ind. Techincal Rev. 48 (2011) 26–32. https://www.mhi.co.jp/technology/review/pdf/e481/e481026.pdf (Accessed 20 August 2018).

[33] R. Haghpanah, R. Nilam, A. Rajendran, Cycle Synthesis and Optimization of a VSA Process for Postcombustion CO_2 Capture, AIChE J. 59 (2013) 4735–4748. doi:10.1002/aic.

[34] S.A. Didas, S. Choi, W. Chaikittisilp, C.W. Jones, Amine-Oxide Hybrid Materials for CO_2 Capture from Ambient Air, Acc. Chem. Res. 48 (2015) 2680–2687. doi:10.1021/acs.accounts.5b00284.

[35] O. Cheung, N. Hedin, Zeolites and related sorbents with narrow pores for CO_2 separation from flue gas, RSC Adv. 4 (2014) 14480–14494. doi:10.1039/C3RA48052F.

[36] M.M. Lozinska, E. Mangano, A.G. Greenaway, R. Fletcher, S.P. Thompson, C.A. Murray, S. Brandani, P.A. Wright, Cation Control of Molecular Sieving by Flexible Li-Containing Zeolite Rho, J. Phys. Chem. C. 120 (2016) 19652–19662. doi:10.1021/acs.jpcc.6b04837.

[37] T.D. Pham, Q. Liu, R.F. Lobo, Carbon Dioxide and Nitrogen Adsorption on Cation-

Exchanged SSZ- 13 Zeolites, Langmuir. 29 (2013) 832–839. doi:10.1021/la304138z.

Highlights

- Li-LSX presented high CO_2/N_2 selectivity in post-combustion conditions
- Limited presence of moisture (1.53 vol%) enhanced CO_2/N_2 selectivity
- Calcination temperature affected CO_2/N_2 selectivity and CO_2 adsorption rate
- Li-LSX outperformed several benchmark adsorbents under post-combustion conditions
- The mechanistic modelling indicated film diffusion as the adsorption limiting step